ANALYSIS OF THE ELECTRICAL CONSUMPTION OF AN AIR-COOLED SINGLE EFFECT AMMONIA/WATER CHILLER

María Esther Palacios-Lorenzo[1], José Daniel Marcos[1]

[1]Dept. of Energy Engineering, Universidad Nacional de Educación a Distancia, UNED, Madrid, (Spain)

Abstract

In this work it is analyzed the effect of the air-coolant flow rate on the absorption chiller performances. With this purpose, a discrete mathematical model has been developed and implemented in Engineering Equation Solver Software, on the bases of mass, species and energy conservation balances. The model has been validated with experimental data of the commercial chiller ROBUR model ACF60-00 LB. Results show that a moderate decrease of the air-coolant velocity may have a positive effect on the chiller performances due to leads to reduce the thermal load of the solution heat exchanger and, simultaneously, the high-level pressure. On the other hand, the electric COP increases due to the marginal decrease in theair-coolant mass flow rate per absorber surface. The drawback is the increase of the absorber size.

Keywords: *air-coolant chiller; ammonia-water; absorption chiller; ASTEP Project; solar cooling*

1. Introduction

Heat supply systems based on absorption heat pump have great potentials on energy saving and emission reduction being able to be powered by waste thermal energy and solar energy, reducing notable electricity consumption. The most common working fluid in absorption refrigeration cycles able to achieve subzero cooling temperatures is the ammonia/water pair. The European ASTEP project is being developed within this framework, and one of its main objectives is to demonstrate the feasibility of the application of solar thermal energy to partially cover the cooling demands at an industrial site, the MANDREKAS dairy company, with a cooling demand at 5ºC. Within that project, the present work aims to study the feasibility and main constrains to use a commercial air-cooled ammonia/water absorption chiller driven by a patented solar concentrator (sun dial) to satisfy the MANDREKAS's cooling demand at different outdoor conditions.

A key feature of the air-cooled absorption chillers is its electrical consumption mainly the amount of air-coolant flow, which should be minimized in order that to be competitive to the vapor compressors of similar cooling capacity (Izquierdo et al., 2012). To evaluate the electrical consumption of the air-cooled chilled when operating in different conditions, the main components of the chiller, namely, distillation column, air-cooled absorber, evaporator and condenser, have been modelled by implementing a discrete model, and subsequently integrated to the whole chiller.

This study analyses the electrical consumption required to cool down the air-cooled absorber and condenser. In particular, the commercial chiller ROBUR model ACF60-00 LB, indirectly fired by pressurized hot water, has been considered.

2. Methods

To study the performance of the single effect air-cooled ammonia/water absorption chiller, a mathematical model has been implemented in Engineering Equation Solver Software, on the bases of mass, species and energy conservation balances (Herold et al. 2016). The material thermal properties have been evaluated from Ibrahim et al (1993). Figure 1 shows a schematic diagram of the chiller. The geometry of the different devices of which the chiller consists, are detailed in Table 1. The distillation column includes a rectifying section and a stripping section, located respectively, above and below of the column feed entry point. A rectifier completes the purification system to achieve vapor refrigerant with a high grade of purity. The lack of appreciable benefits that the rectifying section entails, beside the decrease of COP associated with the use of coupled fluid-cooled rectifier (Fernández-Seara et al., 2002, 2003). and the schematic diagram of the ROBUR (Pereira et al., 2017) justifies considering the purifying system to consist of a distillation column

doi:10.18086/eurosun.2022.08.09 Available at http://proceedings.ises.org

fed from above (only with striping section) helped by a concentrated solution-cooled rectifier to obtain refrigerant vapor of the required purity. On the other side, the refrigerant absorption process in the concentrated solution-cooled absorber has been neglected, being then replaced by the solution heat exchanger.

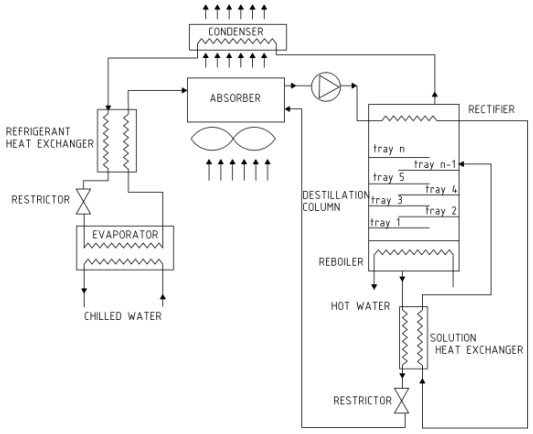

Fig. 1: Schematic diagram of the air-cooled ammonia-water absorption machine

Condenser, absorber, and evaporator tubes are described by its inner diameter, D_i, and thickness, e. The number of tubes is fixed for condenser, absorber, and evaporator, while the tubes length for these devices are obtained in the design process. Conversely, the evaporator tubes length, L, is fixed, while the number of baffles for the chilled water passage is obtained in the design process. The geometry of the finned surface for condenser and absorber, determined by the fin thickness, t_m, hydraulic diameter, D_h, minimum free flow area per frontal area, σ, and heat transfer area to total volume, α, are shown in the table. The reboiler is assumed to be a cylinder equipped externally with annular fins, with the hot water in cross flow over the cylinder, through the resulting fined annuli passage. Geometry of the reboiler annuli finned surface is defined by the length, h_f, thickness, t_m, and pitch, s, of the fins. The distillation column geometry is defined by its inner diameter D_i, hole diameter, d_h=0,00381 m, tray thickness, e_{tray}, tray spacing, S_t, weir length, l_w, hole pitch, s_h=3 d_h, weir height, h_w. and two relationships, f_1 and f_2 (Coker, 2010), being A_t=π/4 D_i^2, A_d, and A_a=A_t-2A_d, the column area, the downcomer area and the active area, respectively.

Table 1. Chiller geometry

Condenser/Absorber		**Distillation column**		**Evaporator**		**Reboiler**	
D_e [m]	0,1638	D_i [m]	0,075	D_i [m]	0.015	h_f [m]	0,01
t_m [m]	0,0004	A_d [m^2]	0,12 A_t	e [mm]	0.002	t_m [m]	0,0004
s [m]	0,00327	S_t [m]	0,15	s [m]	1,15(D_i+e)	s [m]	0,003
D_h [m]	0.0068	h_w [m]	0,1 S_t	N_{tube}	35		
σ	0.499	e_{tray} [m]	0,003	$D_{i,shell}$ [m]	(N_{tube} +1) s		
α [m^2/m^3]	269	A_d/A_t	$f_1(l_w/D_i)$	L [m]	1,1		
N_{tube}	2	A_h/A_a	$f_2(d_h/s_h)$				

Table 2 includes the effectiveness for reboiler, evaporator, condenser and air-cooled absorber, at the design point, required to determine the tubes length of absorber, and condenser, the number of baffles of the evaporator and the height of the reboiler. The effectiveness for these devices is evaluated when the chiller operates at any off-design condition. Conversely, for simplicity, the effectiveness of both internal heat exchangers (solution and refrigerant heat exchangers) is assumed to be constant in every operating condition. In addition, both the ammonia refrigerant mass fraction and the refrigerant quality at the exit of

evaporator are fixed values to limit the refrigerant temperature glide. e_w refers to the weight of the liquid entrainment per unit weight of vapor flowing in the distillation column

Table 2. Chiller parameters

Performance constrictions			**Design point**			
$x_{m,ref}$	0,99		**Coupling fluids temp. change**		**Miscellaneous**	
$Q_{out\ evap}$	0,92		$\Delta T_{cf\ abs}$[C]	1,5	$\dot{Q}_{evap}$[kW]	7,5
e_w	0,05		$\Delta T_{cf\ cond}$ [C]	5	T_{amb} [C]	35
Internal heat exchanger effectiveness	ε_{shx}	0,5	$\Delta T_{cf\ evap}$ [C]	5	$T_{cf\ evap\ out}$ [C]	-5
	ε_{rhx}	0,85	$\Delta T_{cf\ desb}$ [C]	5		

A lumped steady state model has been developed based on the application of global mass, species and energy balance and heat transfer equations and heat exchange effectiveness. The effectiveness of the evaporator, ϵ_e, is defined as (Kim et al. 2008).

$$\epsilon_e = \frac{t_{ei}-t_{eo}}{t_{ei}-T_e} \qquad \text{(eq. 1)}$$

where T and t refer to the temperature of the working fluid and the secondary fluid, respectively. The subscripts i and o refers respectively to the inlet and outlet of the condenser. Therefore, the temperature at the evaporator outlet is calculated as

$$T_e = t_{eo} + \Delta T_{cf\ evap}\left(1 - \frac{1}{\varepsilon_e}\right) \qquad \text{(eq. 2)}$$

being $\Delta T_{cf\ evap}$ the temperature increase suffered by the chilled water as it flows past the evaporator. Similarly, the temperature at the condenser outlet, T_c, may be calculated as

$$T_c = t_{ci} + \frac{\Delta T_{cf\ cond}}{\varepsilon_c} \qquad \text{(eq. 3)}$$

where the effectiveness of the condenser, ϵ_c, is defined as

$$\epsilon_c = \frac{t_{co}-t_{ci}}{T_c-t_{ci}} \qquad \text{(eq. 4)}$$

being $\Delta T_{cf\ evap}$ the temperature increase suffered by the air coolant as it flows past the condenser. In Eqs. (1) and (2), the refrigerant stream is the lowest heat capacity since it undergoes phase change. Note that

$$t_{ci} = T_{amb} + \Delta T_{cf\ abs} \qquad \text{(eq. 5)}$$

where $\Delta T_{cf\ abs}$ refers to the increase of the air coolant temperature as it flows past the absorber. The ammonia mass fraction of both the concentrated, $x_{m\ CS}$, and the diluted solution, $x_{m\ DS}$, is obtained from the reboiler and absorber effectiveness, ϵ_g, ϵ_a, expressed respectively as,

$$\epsilon_g = \frac{T_{go}-T_{gi}}{t_{gi}-T_{gi}} \qquad \text{(eq. 6)}$$

$$\epsilon_a = \frac{T_{ai}-T_{ao}}{T_{ai}-t_{ai}} \qquad \text{(eq. 7)}$$

where the lowest heat capacity is the working stream due to its lower mass flow rate. The temperature of the working fluid at the outlet and inlet of each device is obtained assumed saturated state.

Diluted and concentrated solution flow rates are obtained from the Eqs. (8)-(9) based on mass and species balance in the absorber

$$\dot{m}_s(x_{CS} - x_{DS}) = \dot{m}_r\, x_{CS} \qquad \text{(eq. 8)}$$

$$\dot{m}_{DS} + \dot{m}_r = \dot{m}_{CS} \qquad \text{(eq. 9)}$$

where the refrigerant flow rate, $\dot{m}_r$,is evaluated as

$$\dot{m}_r \approx \frac{\dot{Q}_e}{h_c^{fg}} \qquad \text{(eq. 10)}$$

In addition, the heat transfer rate for absorber or condenser, $\dot{Q}$, is determined with the energy balance, Eq. (11), at the component

$$\dot{Q} + \sum_k \dot{m}_k \cdot h_k = 0 \qquad \text{(eq. 11)}$$

where the solution mass flow rate is denoted by $\dot{m}_k$. The subscript *k* refers to each one of the flows involved in the device. Finally, the mass flow rate of the coupling fluids for evaporator, (chilled water), absorber and condenser (air coolant) are determined.

To determine the reboiler heat transfer rate, the set consist of the reboiler, the purification system and the solution heat exchanger have been modelled. The commercial chiller includes an adiabatic tray type distillation column. Negligible benefit is expected from the rectification section due to its low efficiency (Fernández-Seara et al., 2003). Accordingly, the rectifying section of the distillation column is avoided in the model. Vapor generated in a lower tray experiences liquid-vapor contact with colder solution from the upper tray. The coupled heat and mass transfer process leads to a temperature reduction and purification of the vapor. The liquid flow leaving the tray is assumed to be at thermodynamic equilibrium. Conversely, the ammonia molar fraction of the vapor leaving the i-tray, $\bar{x}_{v,i}$, is obtained calculating the Murphree vapor plate efficiency, e_M. In that way,

$$\bar{x}_{v,i} = \bar{x}_{v,i-1}(1 - e_M) + e_M \bar{x}_{v\,e,i} \qquad \text{(eq. 12)}$$

where $\bar{x}_{v\,e,i}$, refer to the molar fraction of the vapor leaving the i-tray at thermodynamic equilibrium. The Murphree vapor plate efficiency is obtained as

$$e_M = 6.8 \left(N_{R_e} N_{S_c}\right)^{0.1} \left(N_{D_g} N_{S_c}\right)^{0.115} \qquad \text{(eq. 13)}$$

where N_{R_e}, N_{S_c}, N_{D_g} are dimensionless groups depending on some thermodynamic properties of the liquid (σ_L, μ_L, ρ_L, diffusivity of the liquid light key component, evaluated with the Wilke-Chang expression (Coker, 2010), vapor velocity and geometrical characteristics of the column (fractional free area, A_h/A_t, and weir height, h_w). The effect of the liquid entrainment in the Murphree vapor plate efficiency has also been considered by using the Fair method (Coker, 2010). The reboiler Murphree efficiency is assumed to be 1. The vapor purification process is eventually completed by partial condensation in the liquid-cooled rectifier.

Conservation equations for mass, species and energy in every tray are added to the equation set (14)-(25), being reboiler and rectifier considered as additional trays.

Tray without feed:

$$\dot{m}_{L,i+1} + \dot{m}_{V,i-1} = \dot{m}_{L,i-1} + \dot{m}_{V,i+1} \qquad \text{(eq. 14)}$$

$$x_{L,i+1}\dot{m}_{L,i+1} + x_{V,i-1}\dot{m}_{V,i-1} = x_{L,i-1}\dot{m}_{L,i-1} + x_{V,i+1}\dot{m}_{V,i+1} \qquad \text{(eq. 15)}$$

$$h_{L,i+1}\dot{m}_{L,i+1} + h_{V,i-1}\dot{m}_{V,i-1} = h_{L,i-1}\dot{m}_{L,i-1} + h_{V,i+1}\dot{m}_{V,i+1} \qquad \text{(eq. 16)}$$

Reboiler:

$$\dot{m}_{L,1} = \dot{m}_{DS} + \dot{m}_{V,1} \qquad \text{(eq. 17)}$$

$$x_{L,1}\dot{m}_{L,1} = x_{L,i-1}\dot{m}_{DS} + x_{V,1}\dot{m}_{V,1} \qquad \text{(eq. 18)}$$

$$h_{L,1}\dot{m}_{L,1} + \dot{Q}_{reboiler} = h_{PS}\dot{m}_{DS} + h_{V,1}\dot{m}_{V,1} \qquad \text{(eq. 19)}$$

Feed tray:

$$\dot{m}_{L,F} + \dot{m}_{L,i+1} + \dot{m}_{V,i-1} = \dot{m}_{L,i-1} + \dot{m}_{V,i+1} \qquad \text{(eq. 20)}$$

$$x_{L,F}\dot{m}_{L,F} + x_{V,i-1}\dot{m}_{V,i-1} = x_{L,i-1}\dot{m}_{L,i-1} + x_{V,i+1}\dot{m}_{V,i+1} \qquad \text{(eq. 21)}$$

$$h_{L,F}\dot{m}_{L,F} + h_{V,i-1}\dot{m}_{V,i-1} = h_{L,i-1}\dot{m}_{L,i-1} + h_{V,i+1}\dot{m}_{V,i+1} \qquad \text{(eq. 22)}$$

Rectifier:

$$\dot{m}_{V,i-1} = \dot{m}_R + \dot{m}_C \qquad \text{(eq. 23)}$$

$$x_{V,i-1}\dot{m}_{V,i-1} = x_R\dot{m}_R + x_{ref}\dot{m}_{ref} \qquad \text{(eq. 24)}$$

$$\dot{Q}_{rect} + h_{V,i-1}\dot{m}_{V,i-1} = h_R\dot{m}_R + h_C\dot{m}_{ref} \qquad \text{(eq. 25)}$$

where *R*, *C* and *ref* subscripts refer to reflux and vapor refrigerant coming into the condenser, respectively. Subscript *DS* refers to the diluted solution coming out to the reboiler.

2.1. Solution method

The previous formulation may be used in two different ways, namely in the design process of the chiller and as a tool to analyses its off-design performance. In the design process, the value of $\Delta T_{cf\ abs,}$ $\Delta T_{cf\ cond\ ,}$ $\Delta T_{cf\ desb}$ and $\Delta T_{cf\ \ evap}$ are fixed, what lets to determine the length of the condenser and absorber tubes, L_{cond}, $L_{abs,}$ the reboiler heigh, h_{reboil}, and the number of baffles of the evaporator, $N_{baffles}$. In that way, the whole geometry of the chiller may be determined. Chiller performance at off-design conditions may be analysed then, but now $\Delta T_{cf\ abs,}$ $\Delta T_{cf\ cond\ ,}$ $\Delta T_{cf\ desb}$ and $\Delta T_{cf\ \ evap}$ are unknown magnitudes. The solution method for both design chiller and analysis of off-design performances requires an iterative process to match assumed and calculated values for effectiveness of the external heat exchangers and for the temperature change suffered by the corresponding coupling fluid.

Therefore, additional modelling for the external heat exchangers has been developed and implemented. All these models provide the temperature change suffered by the coupling fluid associated with each external heat exchanger. Then, mathematical models for the absorber, condenser, evaporator and reboiler, based on mass, and energy balance, and heat and mass transfer equations, have been developed and implemented. These models are of discrete type for the absorber, condenser and evaporator, and of lumped type for the reboiler. Specifically, the energy balance at the tube solid wall stablishes that

$$\dot{Q}_{l,out} = \dot{Q}_c \qquad \text{(eq. 26)}$$

In Eq. (26), $\dot{Q}_{l,out}$ is the heat flow from the bulk refrigerant to the wall,

$$\dot{Q}_{l,out} = U_{out} \cdot (T_{bL} - T_w) \cdot dA_c \qquad \text{(eq. 27)}$$

where the overall heat transfer coefficient, U_{out}, is given by Eq. (28)

$$U_{out} = \frac{1}{\frac{D_{wo}}{2 \cdot k_w} \ln\frac{D_{wo}}{D_{wi}} + \frac{D_{wo}}{h_{lw} \cdot D_{wi}}} \qquad \text{(eq. 28)}$$

being D_{wi} and D_{wo} the inner and outer tube diameter, respectively. dA_c is the inner heat transfer area from the tube wall to the coolant. h_{lw} refers to the heat transfer coefficient between the liquid phase and the inner tube wall. In addition, $\dot{Q}_c$ is the heat flow transferred from the wall to the air coolant, which is calculated from Eq. (29)

$$\dot{Q}_c = h_{t,c} \cdot \Delta T_{lm} \cdot dA_c \qquad \text{(eq. 29)}$$

being $h_{t,c}$ is the heat transfer coefficient between the wall and the air coolant and ΔT_{lm} the logarithmic mean temperature difference, which is defined as

$$\Delta T_{lm} = \frac{(T_w - T_{ci}) - (T_w - T_{co})}{\ln\frac{T_w - T_{ci}}{T_w - T_{co}}} \qquad \text{(eq. 30)}$$

where the subscripts *ci* and *co* refer to coolant inlet and coolant outlet of the differential control volume, respectively. Eq. (26) lets, known the bulk temperature of the liquid phase, T_{bL}, to obtain T_{co}, and eventually, ΔT_{cf} for each external heat exchanger.

2.1.1 Air-cooled absorber

Bulk temperature of the liquid phase, T_{bL}, is obtained by means of mass, species and energy balance at the vapor and liquid interface. Namely, mass balance at interface, which states than the mass transfer between the vapor and the liquid phases must be equal, can be expressed as Eq. (31), where a film model is used. Eq. (32) is obtained stating a balance energy at the liquid vapor interface (Fernández-Seara et al., 2002, 2003; Sieres et al., 2007)

$$f_1(T_i, z) = 0 \qquad \text{(eq. 31)}$$

$$f_2(T_i, z) = 0 \qquad \text{(eq. 32)}$$

In these equations, *z* refers to the ratio of ammonia to total molar flux through the interface and T_i is the temperature interface. An iterative process leaves to calculate total and partial mass fluxes transferred

through the interface, $\dot{m}$, $\dot{m}_{NH3}$ and $\dot{m}_{H2O}$. New vapor condition is calculated from mass and energy balance in the bulk vapor phase based on the differential control volume, which stablish that

$$d\dot{m}_v = -\dot{m} \quad \text{(eq. 33)}$$

$$d(x_{vb}\dot{m}_v) = -\dot{m}_{NH3} \quad \text{(eq. 34)}$$

$$d(h_{vb}\dot{m}_v) = -\left(\dot{m}_{NH3} \cdot h_{v,NH3} + \dot{m}_{H2O} \cdot h_{v,H2O} + \dot{q}_v\right) \quad \text{(eq. 35)}$$

Similarly, flow rate, temperature and composition of the liquid phase at the exit of the control volume may be obtained with mass balance in the bulk liquid, which states that

$$d\dot{m}_l = \dot{m} \quad \text{(eq. 36)}$$

$$d(x_{lb}\dot{m}_l) = \dot{m}_{NH3} \quad \text{(eq. 37)}$$

$$d(h_{lb}\dot{m}_v) = -\left(\dot{m}_{NH3} \cdot h_{l,NH3} + \dot{m}_{H2O} \cdot h_{l,H2O} + \dot{q}_v\right) \quad \text{(eq. 38)}$$

2.1.2 Condenser and evaporator

Bulk temperature of the liquid phase, T_{bL}, is obtained by means of mass and energy balance at the solution biphasic side.

2.2. Heat and mass transfer coefficients

In the reboiler, the heat transport coefficient between the finned tube wall and the coolant is obtained from (Kay, 1984) and the heat transfer coefficient in the solution side is calculated from Táboas et al., (2007), to consider the mass transfer resistance though the liquid-vapor interface at solution side. The correlation proposed by Klimenko (Mills, 1999) is used between the biphasic refrigerant and the tube surface. In the evaporator, the heat transport coefficient between the tube wall and the coolant is obtained following the procedure described in VDI Heat Atlas (Wärmeatlas, 2010) for the shell-side heat transfer in baffled shell-and-tube heat exchangers. In the condenser and in the absorber, the heat transfer coefficient between the liquid and the tube surface is calculated from the film wise condensation theory in a horizontal tube. In laminar regime, the heat transfer coefficient is obtained from the Nusselt equation for a smooth film (Wärmeatlas, 2010), ignoring the vapor shear stress effect. The increase in heat transfer due to the waviness of the film flow is considered with the Kutateladze and Gogonin equation (Wärmeatlas, 2010). In turbulent regime, the Yüksel and Müller equation (Wärmeatlas, 2010) has been used to calculate the heat transfer coefficient. Corrections proposed by Numrich equations (Wärmeatlas, 2010) have been applied to consider the effect of the shear stress at the condensate film surface, both in laminar and turbulent regime. The heat transport coefficient between the solid surface and the coolant for absorber and condenser has been evaluated by the EES software (7.75-5/8T type) (Kay, 1984). In the absorber, the heat transfer coefficient between the liquid and the liquid vapor interface is assumed to be equal to the heat transfer coefficient between the liquid and the tube wall. The heat transfer coefficient in the refrigerant vapor phase is obtained from Gnielinski (Wärmeatlas, 2010). The mass transfer coefficient is calculated by means of the Chilton and Colburn analogy (Wärmeatlas, 2010) from the heat transfer coefficient.

2.3 Mathematical model validation

The implemented mathematical model has been validated considering the COP and cooling capacity data provided by the manufacture. Note certain discrepancy between experimental data and predicted for chilled water temperature at -5 ^{o}C figure 2 (left) when the outdoor temperature is at 40 ^{o}C. This is attributable to the implemented model is no longer being adequate when the distillation column operates at weep mode, as it may happens when the chiller cooling capacity is very low.

3. Results

The air-coolant absorption chiller, powered by hot water flow, rejects thermal energy from the absorber-condenser assembly to the ambient and so, it can capture energy from the flow water to be chilled in the evaporator. Therefore, the state of the coupling fluids, namely inlet temperature and mass flow rate of the feed water, coolant air and chilled water, determines the performance of the air-cooled absorption chiller. In this work, the inlet temperature of chilled water instead of the outlet temperature is adopted as chiller parameter due to its practical interest. Particularly, the velocity of the air-coolant flow exerts a major influence not only in the size of the absorber-condenser assembly but in the electrical consumption of the chiller.

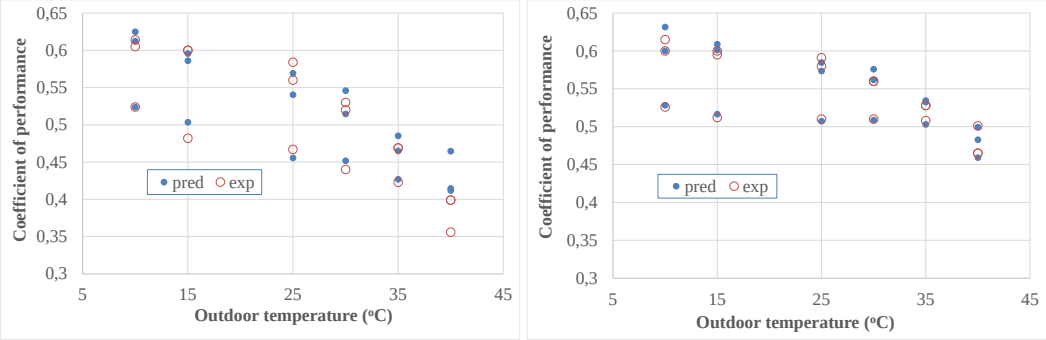

Fig.2: Predicted and manufacture COP data versus outdoor temperature. Hot water mass flow rate: 3500 l/h. Chilled water mass flow rate: 2600 l/h. Hot water temperature: 160, 185 and 240 ºC. Chilled water temperature: -5 ºC (left), 0 ºC (right).

Several cases have been analysed, which characteristics are described in table 1. Firstly, case A is studied. Then, the role of the velocity air-coolant flow is analysed by comparing case B

For each case studied, cooling capacity and COP has been provided by the manufacture, the value of all other significant parameters has been predicted with the implemented model.

Table 3.- Description of the studied cases

	Feed water flowrate (l/h)	**Chilled water flowrate (l/h)**	**Air-coolant velocity (m/s)**	**Chilled water outlet temp. (ºC)**	**Outdoor temp. range (ºC)**	**Feed water temp. range (ºC)**
Case A	3500	2600	2	-5	10-40	160-210
Case B	3500	2600	1	-5	10-40	160-210

3.1. Analysis of the absorber size

The refrigerant absorption in the absorber involves heat and mass transfer processes which rate are partly governed by the absorber thermal resistance, closely related to the air-coolant velocity The refrigerant absorption rate for a variety of working condition has been evaluated. Figure 3 presents the average refrigerant mass flowrate per absorber surface, $\dot{m}_{ref,Aabs}$, when the size of the absorber is the minimum to assure the complete absorption of the refrigerant flow as it passes through the absorber. Similar values were found in water-cooled ammonia-water absorbers (Fernández-Seara et al., 2005). The figure shows that $\dot{m}_{ref,Aabs}$ behaves asymptotically as the air-coolant velocity increases. Therefore, results reveal the existence of a practical maximum for the air-coolant velocity beyond which no further reduction in the absorber size is expected. In this study, the maximum air-coolant flow velocity is set at 2 m/s for the finned surface used to model the absorber.

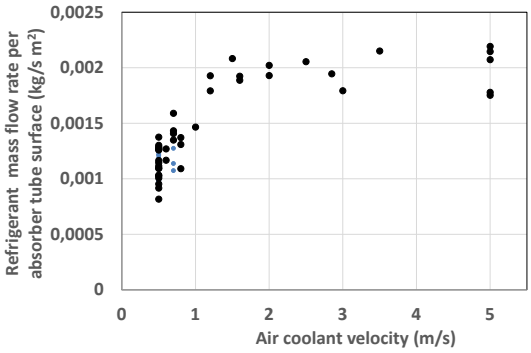

Fig 3: Average refrigerant mass flowrate per solid absorber wall surface versus air coolant velocity.

3.2 Case A

Figure 4 left shows the evolution of the high-pressure level in case A. Note that this magnitude mainly increases as the outdoor temperature does, as expected. Interestingly, it is also increases as the feed water

temperature does. This is attributed to the rise in the cooling capacity, and so, in the thermal load of the absorber. The absorber load influences the condenser performance because they are configured in parallel.

Figure 4 right shows the reflux ratio behaves as the high-pressure level does. This is due to when the high-pressure level increases, the ammonia separation in the reboiler deteriorates as the solution vapor pressure rises.

Figure 5 left presents the effective surface for the condenser, that is, the surface of the where mass transfer processes take place, normalized to its total surface. The condenser effective surface is expected to decrease as the air-coolant mass flow rate increases, due to the heat and mass transfer rate enhancement. In addition, the condenser effective surface increases as the thermal load of the absorber-condenser assembly does, that is, as the cooling capacity increases (or/and the COP decreases). Note the condenser effective surface reaches its higher values when the cooling capacity does.

As regard the electric COP, figure 5 right reveals that it is roughly governed by the outdoor temperature.

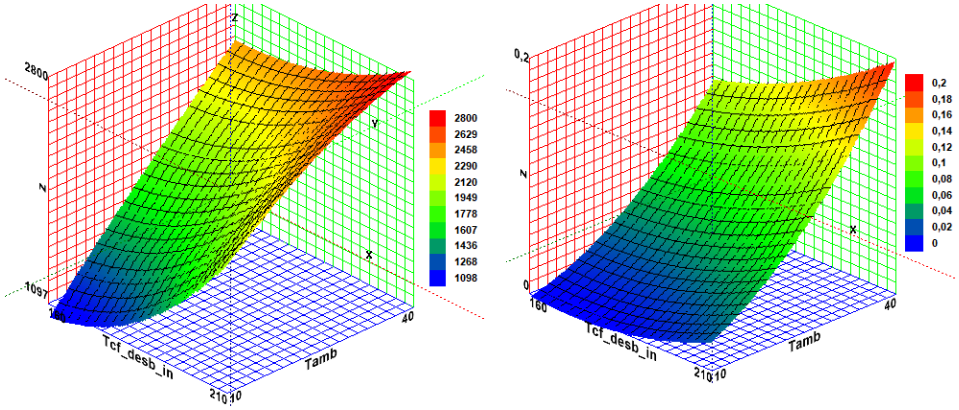

Fig. 4: High-pressure level, in kPa (left). Reflux ratio (right). Case A

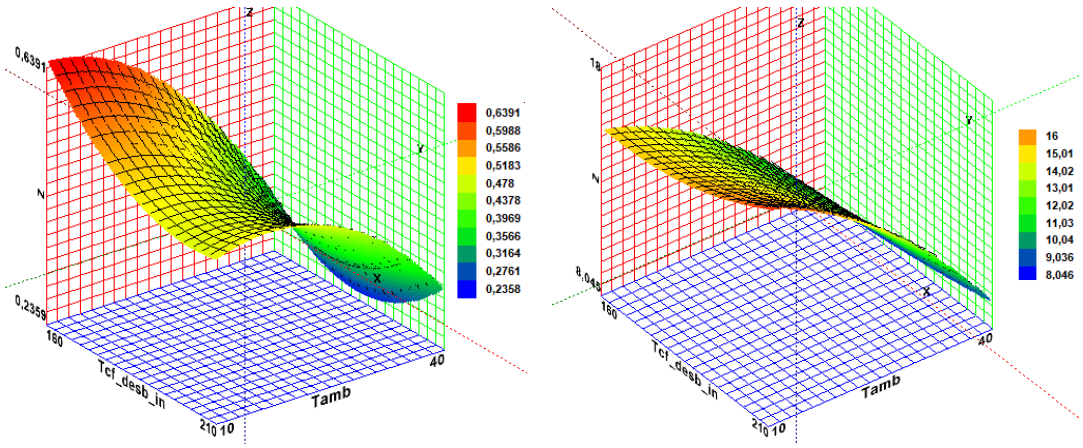

Fig. 5: Condenser effective surface (left). Electric COP (right). Case A

3.3 Case B

Case B characterizes by the fact that the air-coolant velocity is one-half of that one in case A. The distinctive features between case A and B are the followings. Firstly, the high-pressure level has decreased as compared to case A, particularly when the thermal load of the absorber-condenser assembly is maximum. (Figure 6 left). This is a consequence of the decrease in the mass and heat transfer rate. In addition, the thermal load of the solution heat exchanger decreases (Figure 6 right), because of the high-pressure level decrease.

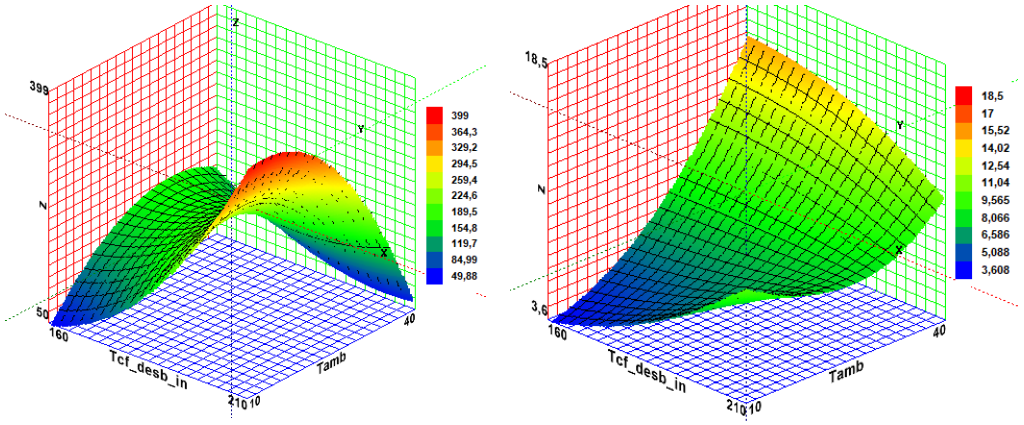

Figure 6: Decrease in the high-pressure level (left), and in the solution heat exchanger thermal load (right), when case B is compared to case A

It is highlighted that the effective surface of the absorber-condenser assembly increases as the air-coolant velocity decreases due to the decay in the mass and heat transfer process (Figure 3). However, the air-coolant mass flowrate increase due to the larger surface of the absorber-condenser assembly is surpassed by the decreases in the air-coolant velocity. Then, figure 7 left shows how the marginal air-coolant mass flow rate per absorber surface decreases in all working conditions. Finally, figure 7 left shows the increases experienced by the electric COP, particularly when the outdoor temperature is low.

4. Conclusion

In this work it is analyzed the effect of the air-coolant flow rate on the absorption chiller performances. With this purpose, a discrete mathematical model has been developed and implemented in Engineering Equation Solver Software, on the bases of mass, species and energy conservation balances. Results show that a moderate decrease of the air-coolant velocity may have a positive effect on the chiller performances due to leads to reduce the thermal load of the solution heat exchanger and, simultaneously, the high-level pressure. On the other hand, the electric COP increases due to the marginal decrease in theair-coolant mass flow rate per absorber surface. The drawback is the increase of the absorber size.

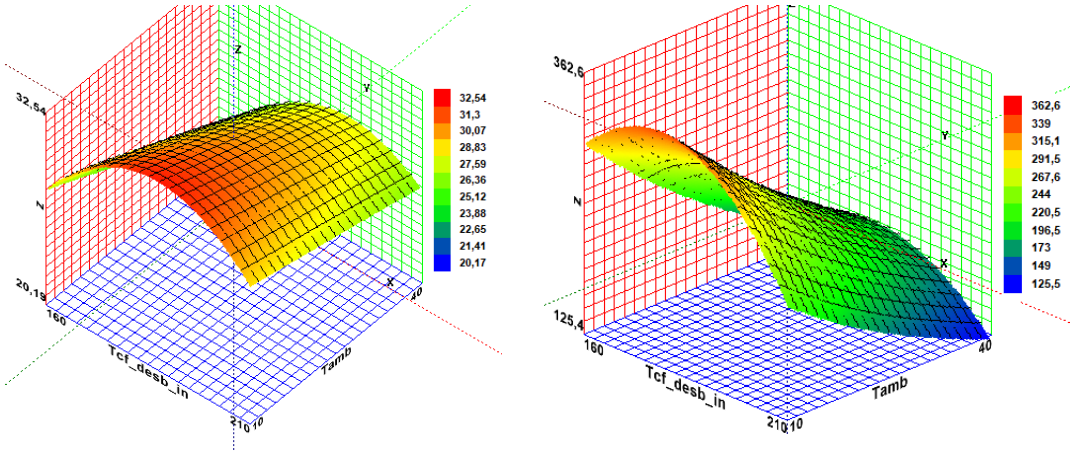

Figure 7: Marginal decrease in the air-coolant mass flow rate per absorber surface, in percentage, (left) and electric COP increases (right) when case B is compared to case A

5 Acknowledgements

This work has been developed in the frame of the ASTEP project, funded by the European Union's Horizon 2020 research and innovation program under grant agreement No 884411 and the ACES2030-CM project, funded by the Regional Research and Development in Technology Program 2018 (ref. P2018/EMT-4319)

6 References

Coker, A. K., 2010. Ludwing's Applied process design for chemical and petrochemical plants. Elsevier, 4th edition

Fernández-Seara, J., J. Sieres, M. Vázquez, 2002. Simultaneous heat and mass transfer of packed distillation for ammonia-water absorption refrigeration systems. Int J. Thermal Sciences, 41, 927-935

Fernández-Seara, J., J. Sieres, M. Vázquez, 2003. Distillation column configurations in ammonia-water absorption chiller refrigeration systems. Int. J. Refrigeration, 26, 28-34

Fernández-Seara, J., J. Sieres, C. Rodríguez, M. Vázquez, 2005. Ammonia–water absorption in vertical tubular absorbers. Int J. Thermal Sciences, 44, 277-288

Herold, K.E., R. Radermacher, S.A. Klein, 2016. Absorption chillers and heat pumps, CRC Press, 2nd edition

Ibrahim, O.M., S.A. Klein, 1993. Thermodynamic properties of ammonia-water mixtures. ASHRAE Trans: Symposia, 21, 2, 1495

Izquierdo M., Marcos J.D., Palacios M.E., González-Gil A., 2012. Experimental evaluation of a low-power direct air-cooled double-effect LiBr-H2O absorption prototype. Energy, 37, 737-748

Kay, W.M., A.L. London, 1984. Compact heat exchangers, McGrawHill, 3rd edition

Kim DS., Infante Ferreira CA., 2008. Analytic modelling of steady state single-effect absorption cycles, Int J. Refrigeration 31, 1012-1020

Mills, A.F., 1999. Transferencia de Calor, McGrawHill, 1st edition

Pereira, J.J., C.A. Cabral, C. Almir, J. Batista, A.A. Ochoa, J.C Charamba, 2017. Energetic analysis of a commercial absorption refrigeration unit using an ammonia-water mixture. Acta Scientiarum, Technology, 39, 439-448

Sieres, J., J. Fernández-Seara, 2007. Modelling of simultaneous heat and mass transfer processes in ammonia-water absorption systems from general correlations. Heat Mass Transfer, 44, 113-123

Táboas, F., M. Vallès, M. Bourouis, A. Coronas, 2007. Pool boiling of ammonia/water and its pure components: comparison of experimental data in the literature with the predictions of standard correlations. Int. J. Refrigeration, 30, 778-788

VDI Wärmeatlas, 2010. VDI Heat Atlas, Springer, 2nd edition

Zamora M., Bourouis M. Coronas A., Vallès M., 2014. Pre-industrial development and experimental characterization of new air-cooled and water-cooled ammonia/lithium bitrate absorption chillers, Int J. Refrigeration 45, 189-197